Time resolved velocity map imaging of methyl elimination from photoexcited anisole

David J. Hadden, Craig A. Williams, G.M. Roberts and Vasilios G. Stavros*

Department of Chemistry, University of Warwick, Coventry, CV4 7AL, UK

*To whom correspondence should be addressed. E-mail: v.stavros@warwick.ac.uk.

Abstract

To date, H-atom elimination from heteroaromatic molecules following UV excitation has been extensively studied, with the focus on key biological molecules such as chromophores of DNA bases and amino acids. Extending these studies to look at elimination of other non-hydride photoproducts is essential in creating a more complete picture of the photochemistry of these biomolecules in the gas-phase. To this effect, CH_3 elimination in anisole has been studied using time resolved velocity map imaging (TR-VMI) for the first time, providing both time and energy information on the dynamics following photoexcitation at 200 nm. The extra dimension of energy afforded by these measurements has enabled us to address the role of $\pi\sigma^*$ states in the excited state dynamics of anisole as compared to the hydride counterpart (phenol), providing strong evidence to suggest that only CH_3 fragments eliminated with high kinetic energy are due to direct dissociation involving a $^1\pi\sigma^*$ state. These measurements also suggest that indirect mechanisms such as statistical unimolecular decay could be contributing to the dynamics at much longer times.

I. Introduction

Photochemistry is everywhere, playing a vitally important role in our day-to-day lives. For example our molecular building blocks readily absorb ultraviolet radiation. However these molecules display a large degree of photostability.[1-3] One of the main reasons for this is that photochemical reactions are effectively quenched through ultrafast non-radiative processes imparting a high degree of photostability to these building blocks of life.[3-5] In light of this, there have been growing efforts both from an experimental and theoretical standpoint, aimed at precisely defining photoresistive pathways potentially operative in some of nature's most important molecules. Recently, dissociative $^1\pi\sigma^*$ states have been implicated as key players in the photoresistive properties of chromophores of aromatic amino acids and DNA bases.[5] Whilst a number of experiments have been directed at searching for spectroscopic evidence of $^1\pi\sigma^*$ states with some success on smaller molecules (e.g. phenol[6-8] and indole,[9-11] the chromophores of the amino acids tyrosine and tryptophan and DNA bases such as adenine[12-14]), the ever-burgeoning question is to what extent do $^1\pi\sigma^*$ states contribute to the photochemistry of a larger range of biological molecules?

The seminal theoretical work of Domcke and Sobolewski originally suggested a general decay pathway that may be common to a number of aromatic and heterocyclic molecules.[5,15] Upon UV irradiation, photon energy is deposited into the molecule through excitation to an optically bright $^1\pi\pi^*$ state. In these molecules, an excited state of $^1\pi\sigma^*$ character intersects, through conical intersections (CIs), both the initially excited $^1\pi\pi^*$ state and the electronic ground state along an X-H stretch coordinate where X is typically O or N. Non-radiative decay along this pathway is predicted to be highly efficient due to the repulsive nature of the $^1\pi\sigma^*$ state leading to

H-atom elimination. Since the prediction of the $^1\pi\sigma^*$ relaxation pathway by *ab initio* calculations an increasing number of experiments have been carried out in the gas phase given the comparison with existing theory which has thus far largely modelled isolated molecules. The $^1\pi\sigma^*$ states, however, are optically dark and their potential energy surfaces (PESs) are dissociative along the X-H coordinate, making them difficult to detect directly, except through time-resolved photoelectron spectroscopy. This is often very challenging, especially as the complexity of the photoelectron spectra increases with increasing molecular size.[16] Instead, characteristics of these states have been exploited for indirect observations. Spectroscopic detection of H-atom appearance times and velocity distributions are indirect evidence for relaxation along the $^1\pi\sigma^*$ state.[17]

Whilst a flurry of both experiment and theory has been directed towards $^1\pi\sigma^*$ states in hydrides, in contrast much less effort has been directed at studying these dissociative states localized on other coordinates such as X-C. The velocity map ion imaging (VMI) work by Ashfold and co-workers was the first to identify the role of $^1\pi\sigma^*$ state induced bond dissociation in non-hydride heteroaromatic systems.[18] Their work on N-methylpyrrole clearly showed the bimodal distribution of CH_3 photoproducts following excitation with UV radiation. In keeping with their H-atom total kinetic energy release (TKER) spectra, the appearance of high and low kinetic energy (KE) components in their spectra were attributed to direct dissociation along the $^1\pi\sigma^*$ state resulting in high KE CH_3 fragments and indirect dissociation, in which highly excited ground state molecules decay, resulting in low KE CH_3 fragments. This work was further complemented by Becucci and co-workers whose combined experimental and theoretical studies showed the existence of two low-lying dissociative $^1\pi\sigma^*$ states localized on the X-CH_3 coordinate in the same system.[19]

Using multi-mass ion-imaging, Ni and co-workers carried out a series of experiments on N-methylindole, N-methylpyrrole and anisole, clearly showing the appearance of either fast or slow CH_3 (or both) fragments following photodissociation at 248 nm and 193 nm, to which they once again rationalized these findings by invoking the presence of a $^1\pi\sigma^*$ state localized on the X-CH_3 coordinate.[20] Most recently, Lim and Kim studied the photodissociation of thioanisole (C_6H_5S-CH_3), observing a striking dependence on the branching ratio between the ground and excited state C_6H_5S fragment (X or A) reaction channels depending on excitation energy.[21]

Although these measurements have provided significant insight into the underlying photophysics of these systems, with clear evidence for the active participation of $^1\pi\sigma^*$ states, very little is known about the timescales of these processes which is critical in unravelling the complex interplay between adiabatic and non-adiabatic dynamics and factors which affect these. In previous studies in phenol-h_6 and phenol-d_5, our group has shown that *both* the high and low KE components of the H-atom KE release spectra indicated appearance timescales in the order of 100 femtoseconds.[8] Whilst this timescale is unsurprising for a direct process in which dissociation occurs within one vibrational period, what is surprising is the timescale for the low KE component, given that this process is expected to be much longer, i.e., once on the electronic ground state, energy must be localized in the correct mode before dissociation can occur (statistical unimolecular decay). This has led us to suggest an alternative decay pathway to generate these low KE H-atoms which is direct. In doing so, this has prompted the work presented here using time-resolved velocity map ion imaging (TR-VMI) studies in anisole in order to compare and contrast the dynamics of this system with its corresponding hydride counterpart (Fig. 1). The work presents strong evidence to suggest that following the same excitation

wavelength as in phenol-d_5 (200 nm) the high KE component of the TKER spectra imply appearance timescales for CH_3 elimination that are ultrafast in contrast to the low KE component. To the best of our knowledge, these are the very first time-resolved measurements of CH_3 elimination which implicate the participation of a $^1\pi\sigma^*$ state, in agreement with recent multi-mass ion-imaging of the same system recorded at 193 nm. Although still speculative, the results presented here also seem to suggest that an indirect route to CH_3 elimination may also be operative at much longer time-delays (~10^2 ps), attributed to a much slower pathway, possibly statistical unimolecular decay.

II. Experimental

For more details regarding the experimental setup, the reader is referred to an earlier publication of ours.[22] The experiments utilize a commercial femtosecond (fs) laser system (Spectra-Physics XP) containing a Ti-Sapphire oscillator and a regenerative amplifier. The amplifier operates at 125 Hz and is centred around 800 nm, delivering 35 fs pulses. The 800 nm output is split into three equally intense beams. The 200 nm pump is obtained by frequency doubling 1 mJ of the fundamental (BBO-type I) and then mixing the 400 nm with residual 800 nm (BBO-type II) to generate 267 nm. The 267 nm is further mixed with residual 800 nm (BBO-type I) to generate approximately 1 μJ/pulse of 200 nm. The remaining two beams are used to pump two optical parametric amplifiers (TOPAS model 4/800/f, Light Conversion). One of the outputs is tunable and is used to provide an alternative, variable-wavelength pump (235 nm – 250 nm) while the other is set at 333.5 nm to probe neutral CH_3-atoms via (2+1) resonance-enhance multi-photon ionization using the

band of the 2-photon $3p\ ^2A_2'' \leftarrow \tilde{X}^2A_2''$ transition,[23] with an output power around 7 μJ/pulse.

The optical delay between the pump and probe is varied over 100 picoseconds (ps) with a minimum step size of 0.025 ps, controlled by a delay stage (Physik-Instrumente). The instrument response function is 170 fs full-width at half-maximum (FWHM), measured through multi-photon ionization of NH_3 and Xe. This is also used to determine time zero (t = 0) for the experiment. A collinear beam of pump and probe pulses is obtained with the help of a dichroic mirror which is focused with the aid of a 500 mm magnesium fluoride lens into the interaction region of a VMI spectrometer to intercept a molecular beam of anisole. The molecular beam is generated by seeding a vapour pressure of anisole (Sigma-Aldrich, $\geq$ 98 %) molecules in He (2-3 atm. and 60 ^oC) and is sent into vacuum using an Even-Lavie pulsed solenoid valve[24] operating at 125 Hz and synchronized to the laser system. Typical opening times of this valve are set to 10-15 μs.

The molecular beam machine consists of a source chamber and interaction chamber, separated by a 2 mm skimmer. The source chamber houses the pulsed valve while the interaction chamber contains the VMI detector, replicating the setup as described by Eppink and Parker,[25] to detect the neutral CH_3 radicals. The CH_3^+ ions are extracted towards the detector by a series of ion optics. The detector consists of a 40 mm diameter Chevron microchannel plate (MCP) assembly coupled to a P-43 phosphor screen (Photek). By applying a timed voltage pulse (Behlke) on the second MCP, we are able to gate on a particular mass ion and record a 2-D CH_3^+ projection by measuring the light emitted from the phosphor screen on a CCD array. The KE spectrum of CH_3-radicals is obtained after the deconvolution of the raw images using an acquisition programme written in LabVIEW implementing the polar onion peeling

method.[26] By measuring the current output directly from the phosphor screen, the setup becomes a time-of-flight mass spectrometer. This enables us to reduce the appearance of clusters by optimizing parameters such as the backing pressure, opening time of the pulsed valve and delay between gas and laser pulses, resulting in an observable reduction in the ion signal of anisole clusters (dimers and trimers etc.) relative to the ion signal of the monomer in the time-of-flight mass spectrum.

III. Results and Discussion

Fig. 2a and 2b shows raw images of CH_3^+ at two pump/probe delays. Fig. 2a corresponds to a delay (t) between the pump (200 nm) and probe (333.5 nm) pulses of +1.5 ps, where the pump precedes the probe while Fig. 2b corresponds to a pump/probe delay of -1.5 ps, the probe now preceding the pump. When the probe precedes the pump, there is considerably less CH_3^+ signal as compared to when the pump precedes the probe (approximately 10 times less total CH_3^+ signal), indicative of a two-colour pump/probe signal in comparison to a combined pump alone and probe alone signal at negative delays. The KE of the CH_3 fragment following dissociation is reflected in the distance of the corresponding CH_3^+ from the centre of the image. In Fig. 2a, there is a small rise in the CH_3^+ signal around 180 pixels from the centre of the image (or 18000 cm^{-1}) that we attribute to CH_3 formed through dissociation via the $^1\pi\sigma^*$ state localized along the O-CH_3 coordinate and is more noticeable in the TKER spectrum shown in Fig. 3 (solid line). The origin of both high and low KE components of the TKER spectrum forms the central discussion of the present work, rationalized in the proceeding paragraphs.

Figure 3 shows the TKER distributions derived from deconvolution of the raw CH_3^+ images and assuming C_6H_5O as the partner fragment, following photoexcitation

at 200 nm and probing through multiphoton ionization at 333.5 nm and 322.5 nm, solid and dashed lines respectively. The delay between the pump and probe pulses was set at 1.5 ps. The spectra are dominated by a low KE component which extends towards high KE. On close inspection of the on-resonance TKER distribution (solid line) one is able to discern a high KE component embedded within the tail of the low KE component, manifested by the noticeable rise in the signal around 18000 cm^{-1}, shaded for clarity. When detuning from the 333.5 nm resonance, the high KE component is significantly reduced, an indication of probing neutral CH_3 through 2+1 REMPI with 333.5 nm following photodissociation.

In recent work on phenol-d_5, which looks at H-atoms eliminated from the O-H group alone,[8] there is a clear bimodal distribution between the low and the high KE components with each component sharing almost equal intensity. In contrast, the on-resonance TKER distribution in Fig. 3 shows a much greater contribution of low KE component as compared to the high KE counterpart. In addition, the high KE component in anisole appears at higher values than the corresponding high KE component in phenol-d_5 following photoexcitation at 200 nm. This is unsurprising given the decrease in the O-CH_3 bond energy (~22500 cm^{-1}) as compared to the O-H bond energy in phenol (~31000 cm^{-1}).[20] The TKER distribution for the on-resonance excitation shown here is in reasonable agreement to that previously reported by Ni and co-workers, the high KE feature peaking in their study ~17000 cm^{-1} compared to ~18000 cm^{-1} measured here. We can estimate the O-CH_3 bond energy from the maximum TKER of the on-resonance distribution in Fig. 3. This value corresponds to 25000 - 26000 cm^{-1} implying the O-CH_3 bond energy is 25000 - 24000 cm^{-1}. This compares reasonably well with the literature value of ~22500 cm^{-1}, the difference likely attributed to the limited resolution of our VMI spectrometer (~1500 cm^{-1} at

these energies) and assuming the phenoxyl radical is formed in its ground vibrational state.

From the on-resonance TKER distribution shown in Fig. 3, it seems unlikely that we are forming both ground state and electronically excited C_6H_5O radicals. The A-state of C_6H_5O lies ~8900 cm^{-1} above the ground state and as such, one would anticipate a difference between the low KE and high KE components to be around this value. The measurements in phenol-d_5 showed this to be so, with the low and high KE components separated by ~9000 cm^{-1}. In anisole, the low and high KE components are separated by ~17500 cm^{-1}, the low KE component peaking around 400 cm^{-1}. One would therefore anticipate an additional peak at ~9000 cm^{-1} (18000 cm^{-1} – 8900 cm^{-1}) which is not immediately apparent in Fig. 3 unless this is buried beneath the tail of the low KE component. As such, the low KE component in anisole peaking at 400 cm^{-1} cannot be attributed to CH_3 with the partner C_6H_5O in the A-state.

Figures 4 and 5 show the first real-time CH_3 elimination in anisole. The transients are shown as a function of pump-probe delay in Fig. 4a, 4b and Fig. 5a, 5b in which the probe was set at 333.5 nm (4a/5a) and 322.5 nm (4b/5b) with insets displaying extended time delays. All four transients are obtained by collecting a series of TKER spectra at various pump-probe delays (t) and integrating each TKER spectrum around the low and high KE features; 230 – 5200 cm^{-1} and 11,500 - 23,000 cm^{-1} respectively for both probe wavelengths. Whilst the dynamics are insensitive to the size of the spectral window in the high KE region (i.e. between 11,500 and 23,000 cm^{-1}), we have chosen a large spectral window for the high KE component for appreciable signal-to-noise. Perhaps the most notable difference in the four transients is the step-like growth of the on-resonance high KE component (Fig. 4a) whilst in the

off-resonance high KE component (Fig. 4b) and low KE component (Figs. 5a and 5b), the signal rises around t = 0 and then decays.

With these measurements, our aim is to obtain appearance timescales for CH_3 elimination and in doing so provide us with detailed information regarding the underlying photochemistry. Most pertinent to this study is whether dissociation occurs directly along the $^1\pi\sigma^*$ state or through some statistical unimolecular decay process on the electronic ground state. From Fig. 3, it is evident that the TKER distribution of the on-resonance high KE component will contain both an on-resonance and off-resonance contribution. As a result, any fitting of the corresponding on-resonance transient shown in Fig. 4a must reflect this. The off-resonance transient shown in Fig. 4b (probe set at 322.5 nm) requires an exponential decay and step function to fit the data (solid blue line) with lifetimes $\tau_{ORdecay} < 65$ fs and $\tau_{ORstep} < 50$ fs, where OR denotes off-resonance. We are unable to quote precise values for $\tau_{ORdecay}$ and τ_{ORstep} given that these timescales are at the limit of our temporal resolution, resulting in large uncertainties in the time-constants. However, both processes are very fast and are likely due to multiphoton excitations that generate CH_3^+ directly, such as: (1) dissociative ionization of the parent ion through a short lived intermediate state accessed by the pump (fast decay) and; (2) pump generated anisole$^+$ (or associated fragment) which is further excited by the probe undergoing dissociative ionization to yield CH_3^+ (fast step).

To fit the on-resonance transient, we have used a combination of the function obtained from the off-resonance transient with an additional step function, to yield a time-constant of $\tau_R = 91 \pm 36$ fs, where R denotes on-resonance. Interestingly, this time-constant is similar to that observed in the hydride counterpart (phenol) which our group measured as $\tau_R = 88 \pm 30$ fs and is very likely indicative of direct dissociation

along the dissociative $^1\pi\sigma^*$ state. The two components of the fit, i.e. the off-resonance component and the step function are shown in Fig. 4a by the blue and red lines respectively. To cross-check the validity of this approach, the amplitudes of the off-resonance component and step function (approximately 1:3 respectively) are in very good agreement with the TKER spectra shown in Fig. 3 - multiplying the high KE component of the off-resonance TKER spectrum by approximately 3 almost overlays the two spectra in the high KE region.

The appearance time of τ_R = 91± 36 fs compared to the hydride counterpart of τ_R = 88 ± 30 fs is much faster than one would anticipate based on the differences in reduced masses of the two systems and peak positions of the high KE features, ~12000 cm^{-1} and ~18000 cm^{-1} in phenol and anisole respectively. Indeed, this would correspond to an almost 3-fold difference between H and CH_3 elimination, i.e. ~ 260 fs for CH_3 elimination. However, one very important factor which determines the time-constant (appearance time) of the fragment being probed is the minimum internuclear separation upon which the fragment can be ionized and detected. Unfortunately, these measurements are unable to determine the internuclear separation beyond which one is able to detect CH_3 (or H) fragments.

Interestingly the low KE transients at the two probe wavelengths are almost identical in comparison to the high KE transients. Figs. 5a and 5b compare the dynamics at probe wavelengths of 333.5 nm and 322.5 nm respectively following excitation at 200 nm. In both cases, the transients are dominated by a rise in the signal close to t = 0 followed by a decay to an elevated baseline. The low KE transients have been obtained by integrating the low KE component (230 – 5200 cm^{-1}) in both the on-resonance and off-resonance KE spectra. It is tempting to fit the low KE CH_3^+ transients with an exponential decay and step function, in much the same way to the

off-resonance high KE component (see Fig. 4b). However, by extending the transients at the two probe wavelengths to longer time-delays, as shown in the insets of Figs. 5a and 5b, there is a clear decay. As a result, in much the same way to the high KE components described above, we have fitted the off-resonance transient shown in Fig. 5b with an exponential decay and step function with lifetimes $\tau_{ORdecay1}$ = 85 ± 15 fs and τ_{ORstep} < 50 fs respectively and a further exponential decay with a lifetime of $\tau_{ORdecay2}$ = 5.9 ± 0.7 ps obtained from the extended transient shown in the inset of Fig. 5b, the subscripts 1 and 2 representing the short and long decay functions respectively. This combined function (solid blue line) is then used to fit the data obtained in the on-resonance low KE transient, keeping the time-constants identical (Fig. 5a). As evident, the fit is very good suggesting that the dynamics of both the on-resonance and off-resonance low KE components, at least at short times, are very similar, if not identical.

We are unable to quantify the exact mechanisms underlying the low KE transient, however this is very likely multicomponent in nature, probably consisting of a multiphoton part giving CH_3^+ directly through dissociative ionization, as evidenced once again by the appearance of CH_3^+ off-resonance. Interestingly two decay components are present, one with a short lifetime (~85 fs) and one with a longer lifetime (5.9 ps - more visible in Fig. 5b) implying that the decay is occurring sequentially through two states, one short lived, the other longer lived. Indeed a decay of 5.9 ps is measured when probing the anisole$^+$ transient, which seems to suggest that this decay is from a short-lived intermediate state in the photoexcited anisole.

Whilst statistical unimolecular decay has thus far been ruled out in the *short* time-transients (0 - 1.5 ps), it is clearly evident that for both the on-resonance low *and* high KE transients collected at *long* time-delays up to 100 ps (insets of Fig. 4a and

Fig. 5a respectively), there is a slow rise in the CH_3^+ signal. Such behavior is absent, within the signal-to-noise, in the off resonance transients (insets of Fig. 4b and Fig. 5b respectively) and is suggestive that CH_3 radicals are being generated through an indirect process such as statistical unimolecular decay following population of the ground state via internal conversion. This may either be through a conical intersection between $^1\pi\sigma^*/S_0$ such as that suggested in the hydride counterpart[27] or some other non-radiative pathway. Alternatively, CH_3 radicals could be formed through fragmentation of the parent anisole$^+$ or highly excited fragments thereof. It is clear from these insets that the timescale for this process is likely to be very long. However we are unable to determine the time-constant of this process with the current setup.

Conclusions

Using TR-VMI, CH_3 radicals are eliminated with a range of KEs following excitation of anisole at 200 nm. The TKER spectrum is dominated by a low KE peak, with a small high KE feature centred around 18000 cm^{-1}. Analysis of the CH_3^+ transients indicates that both the low and high KE components show dynamics on an ultrafast timescale. The dynamics can be modelled using a step function for the high KE component which can be accounted for assuming direct dissociation along the $^1\pi\sigma^*$ state with respect to the O-CH_3 coordinate. The low KE component is likely due to multiphoton processes dominating the dynamics such as dissociative ionization of the parent cation following population of a long-lived state of the parent anisole.

The generalized model for X-H dissociation as suggested by Domcke and Sobolewski seems to apply in non-hydride systems involving a repulsive $^1\pi\sigma^*$ state following photoexcitation with UV light. The timescale for dissociation along this state has been measured as $\tau_R = 91 \pm 36$ fs for CH_3 elimination compared to $\tau_R = 88 \pm$

30 fs for H-atom elimination in phenol. One would anticipate an almost 3-fold difference in the elimination time-scales for the two processes and possibly highlights the point at which CH_3 versus the H can be probed along the O-CH_3 or O-H reaction coordinate respectively. Answers to these questions will no doubt benefit from electronic structure calculations on methylated counterparts in an attempt to correlate the measured dynamics with those predicted from theory.

Acknowledgements

The authors gratefully thank Mr Nicholas Harding for experimental assistance and helpful discussions and Dr Jan Verlet for use of his polar onion peeling program and valuable discussions about VMI. The authors would also like to than Dr Mike Nix for helpful discussions. D.J.H and C.A.W thank the EPSRC for doctoral research fellowships. G.M.R thanks the Leverhulme Trust for postdoctoral funding. V.G.S would like to thank the EPSRC for equipment grants (EP/E011187 and EP/H003401), the Royal Society for a University Research Fellowship and the University of Warwick for an RDF Award.

References

1. P.R. Callis, *Annu. Rev. Phys. Chem.*, 1983, **34**, 329.
2. D. Creed, *Photochem. Photobiol.*, 1984, **39**, 537.
3. C.E. Crespo-Hernández, B. Cohen, P.M. Hare and B. Kohler, *Chem. Re*v., 2004, **104**, 1977.
4. T.J. Martinez, *Acc. Chem. Res.*, 2006, **39**, 119.
5. A.L. Sobolewski, W. Domcke, C. Dedonder-Lardeux and C. Jouvet, *Phys. Chem. Chem. Phys*., 2002, **4**, 1093.
6. M.N.R. Ashfold, A.L. Devine, R.N. Dixon, G.A. King, M.G.D. Nix and T.A.A. Oliver, *Proc. Natl. Acad. Sci. U.S.A.*, 2008, **105**, 12701.
7. C.M. Tseng, Y.T. Lee and C.K. Ni, *J. Chem. Phys.*, 2004, **121**, 2459.
8. A. Iqbal, M.S.Y. Cheung, M.G.D. Nix and V.G. Stavros, *J. Phys. Chem. A*, 2009, **113**, 8157.
9. M.F. Lin, C.M. Tseng, Y.T. Lee and C.K. Ni, *J. Chem. Phys.*, 2005, **123**, 124303.
10. M.G.D. Nix, A.L. Devine, B. Cronin and M.N.R. Ashfold, *Phys. Chem. Chem. Phys*., 2006, **8**, 2610.
11. A. Iqbal and V.G. Stavros, *J. Phys. Chem. A.*, 2010, **114**, 68.
12. H. Satzger, D. Townsend, M.Z. Zgierski, S. Patchovskii, S. Ullrich, and A. Stolow, *Proc. Natl. Acad. Sci. U.S.A.*, 2006, **103**, 10196.
13. M.G.D. Nix, A.L. Devine, B. Cronin and M.N.R. Ashfold, *J. Chem. Phys.*, 2007, **126**, 124312.
14. K.L. Wells, D.J. Hadden, M.G.D. Nix and V.G. Stavros, *J. Phys. Chem. Lett.*, 2010, **1**, 993.
15. A.L. Sobolewski and W. Domcke, *Chem. Phys. Lett.*, 1999, **315**, 293

16. A. Stolow, A.E. Bragg and D.M. Neumark, *Chem. Rev.*, 2004, **104**, 1719.
17. H. Lippert, H.H. Ritze, I.V. Hertel and W. Radloff, *ChemPhysChem.*, 2004, **5**, 1423.
18. A.G. Sage, M.G.D. Nix and M.N.R. Ashfold, *Chem. Phys.*, 2008, **347**, 300.
19. G. Piani, L. Rubio-Lago, M.A. Collier, T.N. Kitsopoulos and M. Becucci, *J. Phys. Chem. A*, 2009, **113**, 14554.
20. C.M. Tseng, Y.T. Lee and C.K. Ni, *J. Phys. Chem. A*, 2009, **113**, 3881.
21. J.S. Lim and S.K. Kim, *Nat. Chem.*, 2010, **2**, 627.
22. K.L. Wells, G. Perriam and V.G. Stavros, *J. Chem. Phys.*, 2008, **130**, 074308.
23. J.W. Hudgens, T.G. DiGiuseppe and M.C. Lin., *J. Chem. Phys.*, 1983, **79**, 571.
24. U. Even, J. Jortner, D. Noy, N. Lavie and C. Cossart-Magos, C, *J. Chem. Phys.*, 2000, **112**, 8068.
25. A.T.J.B. Eppink and D.H. Parker, *Rev. Sci. Instrum.* 1997, **68**, 3477.
26. G.M. Roberts, J.L. Nixon, J. Lecointre, E. Wrede and J.R.R. Verlet, *Rev. Sci. Instrum.*, 2009, **80**, 053104.
27. M.G.D. Nix, A.L. Devine, B. Cronin, R.N. Dixon and M.N.R. Ashfold, *J. Chem. Phys.*, 2006, **125**, 133318.

Figure 1

Molecular structures of a) anisole and b) phenol

Figure 2

Raw images for CH_3^+ following photodissociation of anisole at 200 nm and probing with 333.5 nm. The pump/probe delay was set to +1.5 ps and -1.5 ps in a) and b) respectively.

Figure 3

TKER spectra derived from deconvolution of raw CH_3^+ images and assuming C_6H_5O as the partner fragment, following photoexcitation with 200 nm and probing with a) 333.5 nm (on-resonance) and b) 322.5 nm (off-resonance) radiation. The pump/probe delay was set at 1.5 ps.

Figure 4

CH_3^+ transients as a function of pump (200 nm)/probe delay for high KE CH_3 molecules probed using a) 333.5 nm and b) 322.5 nm respectively. At negative delays, there is no appreciable 2-colour signal. Experimental data in a) and b) were fitted with an off resonance decay and step function with lifetimes $\tau_{ORdecay} < 65$ fs and $\tau_{ORstep} < 50$ fs, respectively and an additional step function in a) with $\tau_R = 91 \pm 36$ fs, where OR and R correspond to off-resonance and on-resonance respectively.

Figure 5

CH_3^+ transients as a function of pump (200 nm)/probe delay for low KE CH_3 molecules probed using a) 333.5 nm and b) 322.5 nm respectively. Experimental data

in a) and b) were fitted with two off-resonance decay functions and a step function having lifetimes of $\tau_{ORdecay1}$ = 85 ± 15 fs, $\tau_{ORdecay2}$ = 5.9 ± 0.7 ps and τ_{ORstep} < 50 fs respectively.

Figure 1

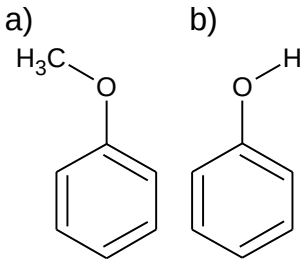

Figure 2

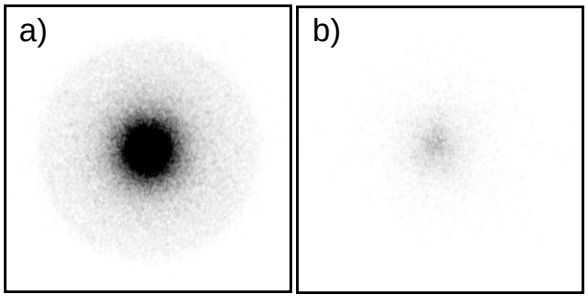

Figure 3

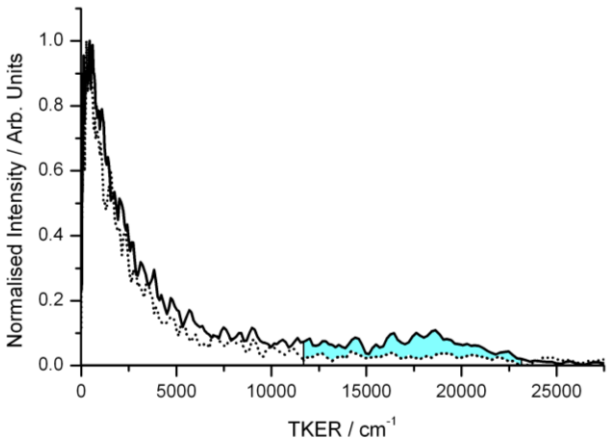
Normalised Intensity / Arb. Units
1.0
0.8
0.6
0.4
0.2
0.0
0
5000
10000
15000
20000
25000
TKER / cm-1

Figure 4

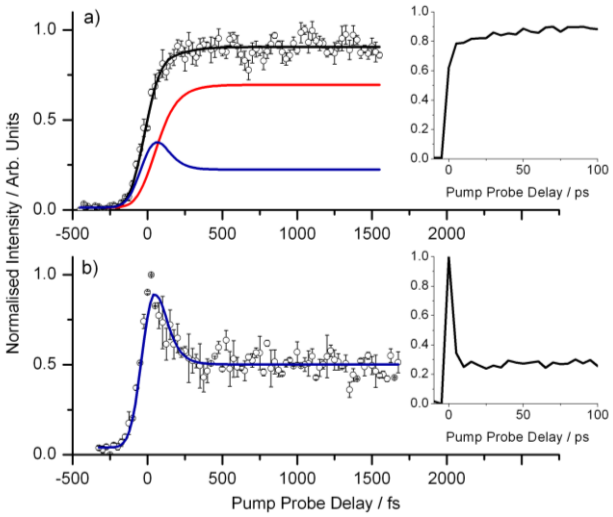
a)
b)
Normalised Intensity / Arb. Units
Pump Probe Delay / fs
Pump Probe Delay / ps
Pump Probe Delay / ps

Figure 5

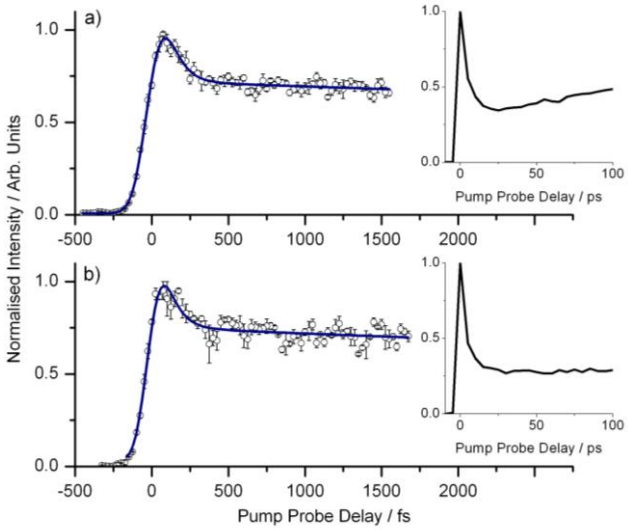
a)
b)
Normalised Intensity / Arb. Units
Pump Probe Delay / fs
Pump Probe Delay / ps
Pump Probe Delay / ps

TOC Figure and Caption:

TR-VMI measurements of methyl elimination from anisole indicate active participation of a $^{1}\pi\sigma^{*}$ state in the photochemistry of anisole.